Available online at www.sciencedirect.com
SCIENCE DIRECT®
Journal of Magnetic Resonance 165 (2003) 293–302
JMR Journal of Magnetic Resonance
www.elsevier.com/locate/jmr

Triple quantum nutation in the two-level NMR system in the rotating frame

Hiroshi Hatanaka,* Manabu Sugiyama, and Noriyuki Tabuchi

Department of Physics, Faculty of Education, Kanazawa University, Kanazawa 920-1192, Japan

Received 23 June 2003; revised 26 August 2003

Communicated by Lucio Frydman

Abstract

The authors present the detailed theory and the new results associated with the triple quantum (TQ) nutation and the line narrowing effect of the TQ resonance in the two-level NMR system which we reported previously. The TQ resonance is induced in the spin-locked system by the oscillating field produced by the sinusoidal phase modulation (PM) of the RF field. The theory predicts that the TQ nutation is accompanied by several higher frequency oscillations and we detected them experimentally by improving the detection system. These higher frequency oscillations are due to the fluctuation of the angle between the transverse or effective field causing the TQ nutation and the RF field. We obtain the result that the modulation index $2\varphi_m$ of the PM is the key parameter that essentially controls the conditions of the TQ resonance and the narrowing effect. Under the exact TQ resonance, the ratio of the TQ resonance frequency to the Larmor frequency of the RF field depends only on φ_m, and the secular part of the magnetic dipole Hamiltonian of a like spin system in the triply rotating frame disappears at a particular value of φ_m. The condition is different from that of the well-known magic angle condition.

Keywords: Multiple quantum NMR; Line narrowing; Double resonance; Magic angle nutation; ^{19}F resonance in Teflon

1. Introduction

The development of line narrowing method is one of the subjects of study which has been attracting large interest in solid NMR. So far, various artificial line narrowing phenomena have been reported, such as magic angle nutation [1], magic angle spinning [2], and the phenomena produced by multiple pulse methods [3].

Recently, we found another type of line narrowing that is produced by a triple quantum (TQ) resonance in a two-level NMR system [4]. The TQ resonance is caused by the cooperation of the rotating and the counter-rotating components of the oscillating field as illustrated in Fig. 1. The TQ resonance induced by the oscillating field at a particular frequency and a particular intensity produces a TQ transient nutation of an extraordinary long decay time. The theory that we have developed to explain the narrowing effect shows that the long decay time is explained by the disappearance of the secular part and the very small nonsecular parts of the magnetic dipole Hamiltonian [4]. This type of narrowing is not a straightforward TQ analog of the usual magic angle narrowing [1].

The theory also shows that the TQ nutation signal is accompanied by some higher frequency oscillations. However, the higher frequency oscillations were not observed in a previous work [4], and also, no observation of such higher frequency oscillations has so far been reported, to our knowledge. The present paper is the first and detailed report on the theoretical and experimental investigations of the higher frequency oscillations. We succeeded in the observation of the higher frequency oscillations by improving the detection system.

The situation that we consider is the TQ resonance of a like nuclear spin 1/2 system which is spin-locked [5,6] by an RF field at exact resonance. The TQ resonance is

* Corresponding author.
E-mail address: hatanaka@ed.kanazawa-u.ac.jp (H. Hatanaka).

1090-7807/$ - see front matter © 2003 Elsevier Inc. All rights reserved.
doi:10.1016/j.jmr.2003.09.005

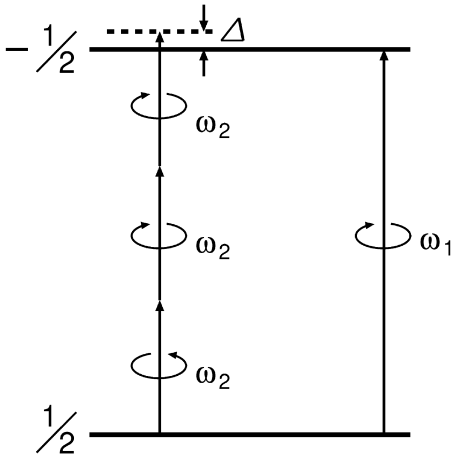

Fig. 1. Energy level diagram of $I = 1/2$ spin system illustrating the mechanism of the TQ resonance. The TQ resonance is induced by three circularly polarized photons of the energy ω_2 (in frequency units) which is nearly equal to one-third of the level spacing ω_1. Each of the two photons corresponds to the normal rotating component of the oscillating field and the other to the counter-rotating component, in this case. Δ indicates the amount of the resultant level shift, which is obtained from Eq. (17). The right arrow means a single quantum transition by a circularly polarized photon of ω_1.

caused in the rotating frame by the oscillating field induced perpendicular to the RF field by the sinusoidal modulation of the RF phase. Under the usual experimental condition, the frequency of the oscillating field is in the range of low frequencies (LF), and therefore, we refer to the oscillating field as an LF field. Since the intensity of the LF field is not so small compared with that of the RF field, the rotating wave approximation is invalid for the LF field; in other words, the counter-rotating component of the LF field becomes effective.

We developed the theory of the TQ resonance with transformations of the density matrix equation of motion to a multiple-rotating frame, which enables us to pictorially understand the spin behaviors in the presence of the LF field. The higher frequency oscillations are interpreted as a result of the fluctuation of the angle between the transverse or effective field causing the TQ nutation and the RF field. Although many theories on the multiple quantum resonance in the two-level system have so far been developed using various approaches [7–9], there are few theoretical developments with several successive transformations to rotating reference frames, to our knowledge. Boscaino et al. [10] used such a kind of transformation method to explain double quantum nutation phenomena. However, our theory is not an extension of theirs because the mechanism of the TQ resonance is different from that of the double quantum resonance, which requires an oscillating field parallel to the predominant static field.

In Section 2, we explain the theoretical approach of the TQ resonance in detail. We obtain the result that the modulation index of the phase modulation (PM) of the RF field is the key parameter that essentially controls the TQ resonance condition and the narrowing condition. In Section 3, the experimental method for the verification of the theoretical approach is described. We use two kinds of methods for settling down of the RF phase after the PM; the one, which is an improved method, is used to verify the present theory, and the other for measuring the decay time of the TQ nutation. The experiments were carried out on ^{19}F nuclei in Teflon. Finally, we present the experimental verifications with some discussions and some comments on the contribution of the magnetic dipole interaction to the TQ nutation decay in Section 4.

2. Basic theory of the TQ resonance

We assume that the spin system $I(=\sum I_j)$ is spin-locked by the RF field $2(\omega_1/\gamma)\cos(\omega_0 t - 2\varphi_m \sin\beta)$ applied perpendicular to the static magnetic field ω_0/γ, where γ is the gyromagnetic ratio of the nuclei and $\beta = \omega_2 t + \varphi$. The total Hamiltonian in the laboratory frame is

$$\mathscr{H}_0(t) = -\omega_0 I_z - 2\omega_1 I_x \cos(\omega_0 t - 2\varphi_m \sin\beta) + \mathscr{H}_d^{(0)} \tag{1}$$

with

$$\mathscr{H}_d^{(0)} = \frac{1}{\hbar}\sum D_{jk}(3I_{jz}I_{kz} - I_j I_k), \tag{2}$$

where D_{jk} is a geometrical factor of a well-known form [11]. We neglect the counter-rotating component of the RF field and the nonsecular part of the magnetic dipolar Hamiltonian as usual under the condition that the static field ω_0/γ is much larger than $2\omega_1/\gamma$ and the local field. To make the normal rotating component of the RF field time-independent, we transform the Hamiltonian $\mathscr{H}_0(t)$ to that in the phase-modulated rotating frame using the unitary operator

$$U_0 = \exp\{-i(\omega_0 t - 2\varphi_m \sin\beta)I_z\}, \tag{3}$$

and obtain

$$\mathscr{H}_1(t) = -\omega_1 I_x - 2\varphi_m \omega_2 I_z \cos\beta + \mathscr{H}_d^{(1)}, \tag{4}$$

where

$$\mathscr{H}_d^{(n)} = U_{n-1}\mathscr{H}_d^{(n-1)}U_{n-1}^{-1}, \quad n = 1, 2, \ldots \tag{5}$$

The PM produces the LF field of the intensity $2\varphi_m\omega_2/\gamma$ at ω_2 perpendicular to the static field ω_1/γ in this rotating frame. Next, we tilt the rotating frame using the operator $U_1 = \exp(i\frac{\pi}{2}I_y)$ and obtain the Hamiltonian in the tilted and phase-modulated rotating frame as

$$\mathscr{H}_2(t) = -\omega_1 I_z + 2\varphi_m \omega_2 I_x \cos\beta + \mathscr{H}_d^{(2)}. \tag{6}$$

We refer to the tilted and phase-modulated rotating frame as an original rotating frame. The spin-locked

magnetization is along the z-axis in the original rotating frame.

Starting from the Hamiltonian $\mathscr{H}_2(t)$, we perform the following series of unitary transformations of the total Hamiltonians. The first transformation is made using $U_2 = \exp(\mathrm{i}\beta I_z)$ to take into account the counter-rotating component of the LF field. The obtained Hamiltonian is

$$\mathscr{H}_3(t) = -(\omega_1+\omega_2)I_z + \varphi_m\omega_2 I_x + \varphi_m\omega_2 \mathrm{e}^{2\mathrm{i}\beta I_z} I_x \mathrm{e}^{-2\mathrm{i}\beta I_z} + \mathscr{H}_d^{(3)}, \tag{7}$$

which is the Hamiltonian in the first rotating frame with respect to the original rotating frame. The first rotating frame rotates at $-\omega_2$, i.e., at ω_2 in the reverse sense to the nuclear precession around the spin-locking field ω_1/γ, in which the effective field ω_e/γ at an angle θ to the field ω_1/γ exists together with the transverse field of the intensity $\varphi_m\omega_2/\gamma$ rotating at $2\omega_2$, where

$$\omega_e = \sqrt{(\omega_1+\omega_2)^2 + (\varphi_m\omega_2)^2}, \tag{8}$$

and

$$\tan\theta = \frac{\varphi_m\omega_2}{\omega_1+\omega_2}. \tag{9}$$

We tilt the first rotating frame using $U_3 = \exp(-\mathrm{i}\theta I_y)$ and obtain

$$\mathscr{H}_4(t) = -\omega_e I_z + \varphi_m\omega_2\cos\theta I_x\cos 2\beta - \varphi_m\omega_2 I_y \sin 2\beta - \varphi_m\omega_2\sin\theta I_z\cos 2\beta + \mathscr{H}_d^{(4)}. \tag{10}$$

If $2\omega_2 \cong \omega_e$, the oscillating transverse fields (in the second and the third terms) cause a resonance in the first rotating frame, which corresponds to the single quantum (SQ) resonance [12] with the Bloch–Siegert shift [13]. However, the angular frequency $2\omega_2$ is sufficiently small compared with ω_e in this case.

We continue the transformation with the operator $U_4 = \exp(-2\mathrm{i}\beta I_z)$, which transforms $\mathscr{H}_4(t)$ to that in the second rotating frame rotating at $2\omega_2$ in the same sense to the nuclear precession around the effective field ω_e/γ. The transformed Hamiltonian is

$$\mathscr{H}_5(t) = -(\omega_e-2\omega_2)I_z + \tfrac{1}{2}\varphi_m\omega_2(1+\cos\theta)I_x - \tfrac{1}{2}\varphi_m\omega_2(1-\cos\theta)\mathrm{e}^{-4\mathrm{i}\beta I_z} I_x \mathrm{e}^{4\mathrm{i}\beta I_z} - \varphi_m\omega_2\sin\theta I_z\cos 2\beta + \mathscr{H}_d^{(5)}, \tag{11}$$

which indicates that, in the second rotating frame, there exists the second effective field ω_e^*/γ at an angle α to the effective field ω_e/γ accompanied by the rotating and the oscillating fields, where ω_e^* and α are, respectively, given by

$$\omega_e^* = \sqrt{(\omega_e-2\omega_2)^2 + \left[\tfrac{1}{2}\varphi_m\omega_2(1+\cos\theta)\right]^2} \tag{12}$$

and

$$\tan\alpha = \frac{\frac{1}{2}\varphi_m\omega_2(1+\cos\theta)}{\omega_e-2\omega_2}. \tag{13}$$

The Hamiltonian $\mathscr{H}_5(t)$ is furthermore transformed by the operator $U_5 = \exp(-\mathrm{i}\alpha I_y)$ to

$$\mathscr{H}_6(t) = -\omega_e^* I_z - 2\omega_3 I_x\cos 2\beta - \varphi_m\omega_2\sin\theta\cos\alpha I_z\cos 2\beta + \tfrac{1}{2}\varphi_m\omega_2(1-\cos\theta)\sin\alpha I_z\cos 4\beta - \tfrac{1}{2}\varphi_m\omega_2(1-\cos\theta)\cos\alpha \mathrm{e}^{-4\mathrm{i}\beta I_z} I_x \mathrm{e}^{4\mathrm{i}\beta I_z} - \tfrac{1}{2}\varphi_m\omega_2(1-\cos\theta)(1-\cos\alpha)I_y\sin 4\beta + \mathscr{H}_d^{(6)}, \tag{14}$$

where

$$\omega_3 = \tfrac{1}{2}\varphi_m\omega_2\sin\theta\sin\alpha. \tag{15}$$

We now make some approximations as follows under the condition that the angles θ and α are small. Since the static term $-\omega_e^* I_z$ is regarded as an unperturbed Hamiltonian in this reference frame, the third and the fourth terms showing the interactions of the spin system with the oscillating fields along the static field ω_e^*/γ can be neglected. The fifth and the sixth terms indicate the interactions with the field that rotates inversely with respect to the nuclear precession around the second effective field ω_e^*/γ and with a very weak oscillating field, respectively. Therefore, these time-dependent terms are negligible even if $4\omega_2 \cong \omega_e^*$. Thus, the most probable resonance is produced by the second term when $2\omega_2 \cong \omega_e^*$.

We mainly consider the case

$$2\omega_2 = \omega_e^*. \tag{16}$$

We may call the resonance a TQ resonance because ω_2 satisfying Eq. (16) becomes $\frac{1}{3}\omega_1$ at the limit of $\varphi_m = 0$. Hereafter, ω_2 satisfying Eq. (16) is denoted by ω_{20}. The explicit expression of ω_{20} is complicated. The ratio ω_1/ω_{20} is obtained approximately from Eq. (16), using a mathematical computer program "maple 7," as

$$\frac{\omega_1}{\omega_{20}} = 3 - \frac{3}{8}\varphi_m^2 - \frac{9}{512}\varphi_m^4. \tag{17}$$

The second and the third terms in Eq. (17) present the shift of ω_{20} from $\omega_1/3$ (corresponds to $\Delta/3$ in Fig. 1). Eq. (17) is consistent with theoretical results derived by Ahmad and Bullough [8] and Swain [9].

The effects of the TQ resonance are described with the following static Hamiltonian in the third reference frame rotating at $2\omega_{20}$ around the second effective field ω_e^*/γ,

$$\mathscr{H}_7 = -\omega_3 I_x + \bar{\mathscr{H}}_d^{(7)} \tag{18}$$

which is obtained by transforming with $U_6 = \exp(-2\mathrm{i}\beta I_z)$, where $\bar{\mathscr{H}}_d^{(7)}$ is the time-independent part of $\mathscr{H}_d^{(7)}$. We neglect the counter-rotating component of the resonant oscillating field in the second term in Eq. (14) and the oscillating terms of $\mathscr{H}_d^{(7)}$. The third rotating frame rotates triply with respect to the original rotating frame as illustrated in Fig. 2. We here consider the angles ξ_x, ξ_y, and ξ_z that the x-, the y-, and the z-axes of the triply rotating frame make with the field ω_1/γ, where the

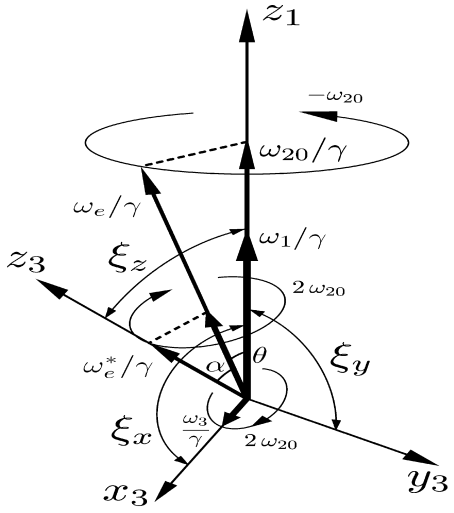

Fig. 2. Schematic illustration of the triply rotating frame. The first effective field ω_e/γ at an angle θ to the RF field along the z_1 axis rotates at an angular frequencyof $-\omega_{20}$ around the RF field in the original rotating frame. The second effective field ω_e^*/γ at an angle α to the field ω_e/γ rotates at $2\omega_{20}$ around ω_e/γ, and the transverse field ω_3/γ causing the TQ nutation rotates at $2\omega_{20}$ around ω_e^*/γ. The notations ξ_x, ξ_y, and ξ_z mean the angles that the x_3, y_3, and z_3 axes of the triply rotating frame make with the RF field.

x- and the z-axes are taken along the transverse field ω_3/γ and the second effective field ω_e^*/γ, respectively. (These axes are denoted by x_3, y_3, and z_3 in Fig. 2.) The field ω_1/γ is parallel to the z-axis of the original rotating frame (denoted by z_1). Since the angle ξ_x is not so different from $\pi/2$ for the small values of θ and α, the nutation of the magnetization initially along the field ω_1/γ can be sufficiently caused around the transverse field ω_3/γ (the TQ nutation) and observed through the oscillation of the component M_z of the magnetization along the field ω_1/γ in the original rotating frame, if the field ω_3/γ is large enough compared with the local field due to $\bar{\mathscr{H}}_d^{(7)}$.

However, the time development of $M_z(t)$ includes higher frequency oscillations because the angles ξ_r's $(r = x, y, z)$ depend on time as seen from Fig. 2. The angle ξ_z fluctuates at a frequency of $2\omega_{20}$ owing to the rotation of the second effective field ω_e^*/γ, where the rotation of the first effective field ω_e/γ does not affect on the fluctuation of ξ_z because it rotates at a constant angle θ around the z_1-axis. Therefore, the angle ξ_x fluctuates by virtue of the fluctuation of ξ_z and the rotation of the field ω_3/γ at $2\omega_{20}$ around ω_e^*/γ, as a result, $M_z(t)$ oscillating at ω_3 fluctuates with frequencies $2\omega_{20}$ and $4\omega_{20}$.

The time development of $M_z(t)$ is calculated with

$$M_z(t) = \mathrm{Tr}\{I_z V(t)^{-1} e^{-i\bar{\mathscr{H}}_7 t} V(0)\rho(0) V(0)^{-1} e^{i\bar{\mathscr{H}}_7 t} V(t)\}, \tag{19}$$

where $V(t) = U_6 U_5 U_4 U_3 U_2$, and

$$\rho(0) = 1 + I_z M_z(0)/\mathrm{Tr}(I_z^2) \tag{20}$$

which is the initial density matrix of the spin system in the original rotating frame under the high temperature approximation. In the calculation of $M_z(t)$, we replace $\bar{\mathscr{H}}_d^{(7)}$ by its secular part $\mathscr{H}_d^{\dagger}$ as usual, which is the static part of $e^{-i\omega_3 I_x t}\bar{\mathscr{H}}_d^{(7)} e^{i\omega_3 I_x t}$. Although the explicit expression of $M_z(t)$ is complicated, we can express it in a compact form as

$$\begin{aligned} M_z(t) = {} & M_z(0)\cos\xi_x(0)\cos\xi_x(t) \\ & + M_z(0)|\sin\xi_x(0)|\Gamma(t)[\cos\xi_z(t)\cos(\omega_3 t + \psi) \\ & + \cos\xi_y(t)\sin(\omega_3 t + \psi)], \end{aligned} \tag{21}$$

using the relation,

$$V(t) I_z V(t)^{-1} = \cos\xi_x(t) I_x + \cos\xi_y(t) I_y + \cos\xi_z(t) I_z, \tag{22}$$

where,

$$\begin{aligned} & \Gamma(t) = \mathrm{Tr}\{e^{-i\mathscr{H}_d^{\dagger} t} I_z e^{i\mathscr{H}_d^{\dagger} t} I_z\}/\mathrm{Tr}(I_z^2), \\ & \tan\psi = \cos\xi_y(0)/\cos\xi_z(0). \end{aligned} \tag{23}$$

The validity of Eq. (22) is understood by noting that I_r's $(r = x, y, z)$ in the right-hand side of Eq. (22) are the spin operators in the triply rotating frame, whereas I_z between the operators V and V^{-1} in the left-hand side is in the original rotating frame.

The first term in Eq. (21) shows the behavior of the component of the magnetization $M_z(0)\cos\xi_x(0)$ along the transverse field ω_3/γ (the TQ spin-locked magnetization) and the second one that of the component perpendicular to ω_3/γ $[M_z(0)|\sin\xi_x(0)|]$. The values of $\cos\xi_r(0)$'s $(r = x, y, z)$ obtained from Eq. (22) depend on θ, α, and φ. The angles θ and α depend on φ_m and ω_1/ω_{20} as seen from Eqs. (9) and (13), and the resonance condition (16) presents the relation between φ_m and ω_1/ω_{20} [see Eq. (17)]. Therefore, the angles θ and α at the exact resonance depend only on φ_m and the values of $\cos\xi_r(0)$'s are determined only by φ_m and φ. Rearranging the right-hand side of Eq. (21) with the explicit expressions of $\cos\xi_r(t)$'s, we can see that the time development of $M_z(t)$ consists of seven simple harmonic oscillations and a static term. An example of the theoretical time development of $M_z(t)$ is shown in Fig. 3, which is obtained at $\varphi = 0$. The leftmost line of the Fourier spectrum in the lower figure corresponds to the TQ nutation and the other ones to the higher frequency oscillations. The oscillations corresponding to the leftmost line (at ω_3) and four weak lines (at $2\omega_{20} \pm \omega_3$ and $4\omega_{20} \pm \omega_3$) come from the second term of Eq. (21), and therefore, decay according to $\Gamma(t)$. On the other hand, the oscillations corresponding to the strong lines at $2\omega_{20}$ and $4\omega_{20}$ originate in the first term of Eq. (21), which do not show the decay due to $\Gamma(t)$. Although the oscillation signal in Fig. 3 is at the exact resonance, $M_z(t)$ includes a small static magnitude due to the static term in the first term of Eq. (21).

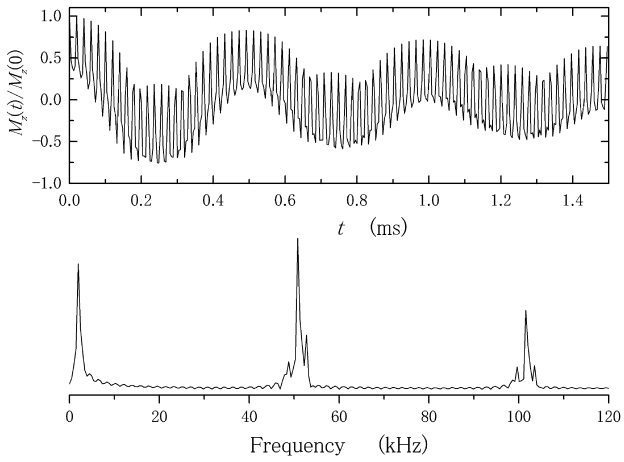

Fig. 3. Theoretical time development of $M_z(t)$ produced during the PM and its Fourier spectrum. The time development is obtained under the condition that $\omega_1/2\pi = 65\,\text{kHz}$, $\omega_{20}/2\pi = 25.41\,\text{kHz}$, $\varphi_m = 1.057\,\text{rad}$, and $\varphi = 0$, using the exponential decay function with $T = 1.1\,\text{ms}$. The leftmost line in the lower figure corresponds to the TQ nutation frequency $\omega_3/2\pi = 1.98\,\text{kHz}$. Three lines around 50 kHz are at the frequencies of $2\omega_{20}$ and $2\omega_{20} \pm \omega_3$, and those around 100 kHz at $4\omega_{20}$ and $4\omega_{20} \pm \omega_3$.

We next comment on the dipole Hamiltonian $\bar{\mathscr{H}}_d^{(7)}$. The calculation of $\bar{\mathscr{H}}_d^{(7)}$ with the well-known tensor operators $T_{2q}(q = -2 \sim 2)$ [3] leads to the result

$$\bar{\mathscr{H}}_d^{(7)} = \sum D_{jk}[A(3I_{jz}I_{kz} - I_jI_k) + B(I_{jx}I_{kx} - I_{jy}I_{ky}) + C(I_{jx}I_{kz} + I_{jz}I_{kx})], \tag{24}$$

with

$$\begin{aligned} A &= -\tfrac{1}{32}(1 + 3\cos 2\theta)(1 + 3\cos 2\alpha) + \tfrac{3}{16}(\sin 2\theta + 2\sin\theta)\sin 2\alpha, \\ B &= -\tfrac{3}{32}(1 - \cos 2\theta)(1 - \cos\alpha)^2 - \tfrac{3}{32}(\sin 2\theta - 2\sin\theta)(\sin 2\alpha - 2\sin\alpha), \\ C &= +\tfrac{9}{32}(1 - \cos 2\theta)\sin 2\alpha - \tfrac{3}{32}(1 + \cos\theta)^2(\sin 2\alpha - 2\sin\alpha) - \tfrac{3}{8}\sin 2\theta(\cos 2\alpha - \cos\alpha). \end{aligned} \tag{25}$$

The secular part $\mathscr{H}_d^{\dagger}$ of $\bar{\mathscr{H}}_d^{(7)}$ and the nonsecular part $\mathscr{H}_d^{\ddagger} \equiv \bar{\mathscr{H}}_d^{(7)} - \mathscr{H}_d^{\dagger}$ are given by

$$\mathscr{H}_d^{\dagger} = \tfrac{1}{2}(B - A)\sum D_{jk}(3I_{jx}I_{kx} - I_jI_k), \tag{26}$$

and

$$\mathscr{H}_d^{\ddagger} = \sum D_{jk}[-\tfrac{1}{2}(3A + B)(I_{jy}I_{ky} - I_{jz}I_{kz}) + C(I_{jx}I_{kz} + I_{jz}I_{kx})]. \tag{27}$$

The coefficient $(B - A)/2$ is equivalent to K in a previous work [4]. The coefficients A, B, and C are also determined only by φ_m under the condition of exact resonance. At $\varphi_m \cong 1.16322\,\text{rad}$, $A = B$, namely the secular part vanishes, where φ_m at which $A = B$ is denoted by φ_{m0}. The value of B is almost 0 in the range of $\varphi_m = 0$–$1.5\,\text{rad}$. Therefore, at φ_{m0}, the value of $|3A + B|/2$ is also nearly equal to 0 ($\cong 2.44 \times 10^{-3}$) and the nutation decay is essentially due only to the second term of $\mathscr{H}_d^{\ddagger}$ with the coefficient $|C| = 0.23079$.

3. Experimental method

The experiment was performed with the RF field at the frequency $\omega_0/2\pi = 27\,\text{MHz}$ on ^{19}F nuclei in Teflon at room temperature, using home-made NMR equipment. After the nuclear magnetization was aligned along the RF field by a standard spin-locking procedure [6], we applied the PM to the RF field using an LF oscillator (HP 33120A) with a function of burst modulation as illustrated in Fig. 4. The LF signal generated by the LF oscillator was fed to the phase modulator of the RF oscillator (ANRITSU MG443B) through the gated LF amplifier. When the sample coil was tuned best, the smallest amplitude modulation (AM) at the frequency $2\omega_2$ was produced in the RF field. The amplitude of the AM was 5% or less of that of the RF field, but its effect on the TQ resonance phenomena could be quite neglected. The degree of modulation index $2\varphi_m$ was measured from an oscillation pattern observed by mixing two RFs at the same frequency with and without the PM through a doublebalanced mixer (DBM).

The TQ resonance phenomena were observed by plotting the magnitude of the M_z detected after the spin-locking pulse as a function of ω_2 or the duration of the PM pulse. The spin locking pulse is followed by a $\pi/2$ pulse with the same RF phase, after which a solid echo is induced [14]. The magnitude of M_z is measured from the defocusing part of the solid echo signal. When we change the duration of the PM, the delay time t_d of the PM pulse and the time margin t_m of the RF field after the PM pulse are kept constant. The durations of t_d and

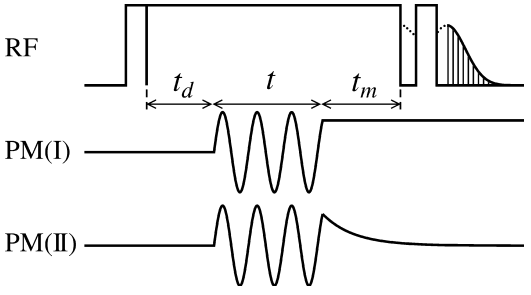

Fig. 4. Operation for the experiments on the TQ resonance. The top trace illustrates the standard pulse sequence for the spin locking followed by the $\pi/2$ pulse with the same phase as the second pulse. The last pulse is applied to detect a kind of solid echo signal. The defocusing part of the echo signal is adopted as the magnitude of M_z. The separation between the second and the last pulses corresponds to the dead time of the receiver amplifier (about 15 μs). The middle and the bottom traces indicate the PMs of the RF field. The PM(I) and the PM(II) are used for the verification of the theory and the measurements of the decay times of the TQ nutation, respectively.

t_m are about 300 and 500 μs, respectively, which are sufficiently long compared with the decay time of the conventional nutation around the RF field. We applied the PM not only to the RF field but also to the reference signal for the phase sensitive detection. We adopted two kinds of methods for settling down the RF phase after the PM pulse (see Fig. 4). In the method I [PM(I)], the RF phase is kept constant in order to detect the solid echo signal at the RF phase just after the PM pulse. By this method, the time developments of $M_z(t)$ are observed in the original rotating frame and can be compared with the theoretical results. In the method II [PM(II)], we gradually change the RF phase to zero in a duration of about 100 μs. We used the method II for the measurements of nutation decay times because it considerably decreases the higher frequency oscillations superposed on the nutation signal.

The intensity of the RF field was adjusted mainly so that $\omega_1/2\pi = 65$ kHz by measuring the center frequency of the usual rotary saturation curve [15] with a weak LF field, where ω_2 was varied under the conditions of the constant amplitude of the LF field $2\varphi_m\omega_2/\gamma$ and the constant duration of the PM pulse ($\cong$3 ms). The resonance frequency $\omega_{20}/2\pi$ was measured from the TQ saturation curve observed for the relevant amplitude of the LF field with a PM pulse of the duration of about 4 ms. We used an averaging method similar to that used in a previous work [16] to reduce the contribution of the higher frequency oscillations to the TQ saturation curve. In case a small fluctuation appeared on the saturation curve due to the higher frequency oscillations and the tail of the transient nutation signal, we removed it with a computer program of an FFT filter. The circles in Fig. 5 show the experimental values of ω_{20} thus obtained for $\omega_1/2\pi = 65$ kHz, which are in good agreement with the theoretical ones (solid line) calculated with Eq. (16) or Eq. (17).

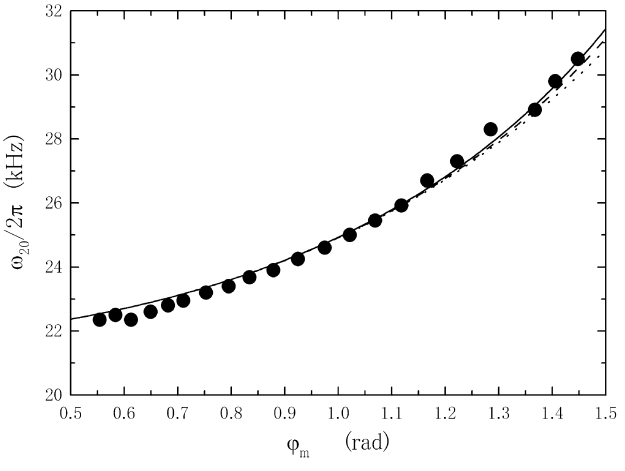

Fig. 5. Dependences of the TQ resonance frequency ω_{20} on φ_m. The circles show the experimental values of ω_{20}. The solid line is our theoretical result obtained with Eq. (17) for $\omega_1/2\pi = 65$ kHz. The curve is almost the same as that obtained from Eq. (16). The broken and the dotted lines are the theoretical results by Ahmad and Bullough and by Swain, respectively.

A 300-W RF amplifier (THAMWAY A55-3602MR) produced a strong RF field in the sample coil of 15-mm diameter and 18-mm length. A sample whose volume was about 1/80 of that of the sample coil was used to reduce the effect of inhomogeneity of the RF field.

4. Experimental verifications and discussion

4.1. TQ nutation

The experimental verification of the time development of $M_z(t)$ in Fig. 3 is shown by the top and middle figures of Fig. 6. The Fourier spectrum of time development (the middle figure) is in good agreement with the theoretical one if the lines near ω_{20} and $3\omega_{20}$ are

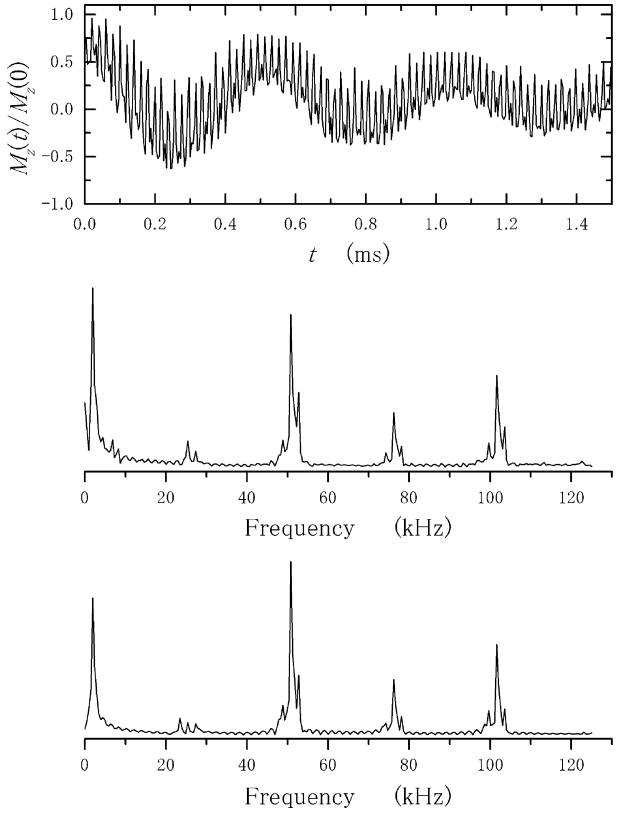

Fig. 6. Experimental time development of M_z (top) and its Fourier spectrum (middle) corresponding to those in Fig. 3. The leftmost line and the other lines in the middle figure indicate the TQ nutation frequency (1.95 kHz) and the frequencies of the higher frequency oscillations. The experimental condition is $\omega_1/2\pi = 65$ kHz, $\omega_{20}/2\pi = 25.41$ kHz, $\varphi = 0$, and $\varphi_m = 1.071$ rad. The lines around ω_{20} and $3\omega_{20}$ that are not seen in Fig. 3 are explained to be due to the oscillations of transverse magnetization. The bottom figure shows the theoretical Fourier spectrum corresponding to the experimental one, which is obtained by assuming that M_z is mixed with the magnitude of $0.2M_x$ in the original rotating frame at the end of the PM pulse.

ignored. However, these unexpected lines are not negligibly small. It cannot be considered that these lines are due to the oscillating terms neglected in Eq. (14), because their frequencies are $2\omega_{20}$ or $4\omega_{20}$. The most probable cause of these lines is the mixing of M_z with the transverse component (perpendicular to M_z) in the original rotating frame. The time development of M_x, for example, is described by the equation modified from Eq. (21) by replacing only the time-dependent angles $\xi_r(t)$'s $(r = x, y, z)$ by the angles $\sigma_r(t)$'s defined by

$$V(t)I_xV(t)^{-1} = \cos\sigma_x(t)I_x + \cos\sigma_y(t)I_y + \cos\sigma_z(t)I_z. \tag{28}$$

The angle σ_r t, which is the angle between the r-axis in the triply rotating frame and the x-axis in the original rotating frame, is under the influence of the rotation of the first effective field ω_e/γ. Therefore, the time development of M_x consists of the oscillations around ω_{20}, $3\omega_{20}$, and $5\omega_{20}$. The same holds for M_y. However, the transverse component should almost disappear during the time margin t_m of the RF pulse. Probably, M_z is mixed with a part of the transverse component by a momentary turbulence of the RF phase at the end of the PM pulse. The bottom figure of Fig. 6 is the Fourier spectrum of the theoretical time development of M_z mixed with a magnitude of $0.2M_x$, the pattern of which resembles the experimental one very well.

Eq. (21) and also the corresponding equations for M_x and M_y indicate that the initial phase φ affects largely the amplitudes of the respective simple harmonic oscillations through the angle $\xi_x(0)$. From Eq. (22), the representative values of $\xi_x(0)$ are obtained as $\pi/2 - (\theta + \alpha)$ at $\varphi = 0$, $\pi/2 + \theta$ at $\varphi = \pi/4$, and $\pi/2 + (\alpha - \theta)$ at $\varphi = \pi/2$. At $\varphi = 0$, the value of $\cos\xi_x(0)$ is the largest, and therefore, the amplitudes of the oscillations exactly at $n\omega_{20}$ $(n = 1$–$5)$ are maximum. Actually, the intensities of the center lines at $2\omega_{20}$, $3\omega_{20}$, and $4\omega_{20}$ in Fig. 6 were larger than those observed for any other degree of φ. (We could not confirm such φ dependences for the lines at ω_{20} and $5\omega_{20}$ because of their weak intensities.) As expected from the representative values of $\xi_x(0)$, $\xi_x(0)$ becomes $\pi/2$ at a value of φ between 0 and $\pi/4$. The disappearances of the higher frequency oscillations exactly at $n\omega_{20}$ $(n = 1$–$4)$, indicating that $\xi_x(0) = \pi/2$, were observed at about $\varphi = \pi/6$ for $\varphi_m = 1.07$ rad. The other characteristics of the higher frequency oscillations were also experimentally confirmed. For example, when the lines exactly at $n\omega_{20}$ $(n = 1$–$4)$ became strong, the other ones, including that at ω_3, became weak.

The φ dependence of $\xi_x(0)$ enables us to reduce the higher frequency oscillations by averaging the several magnitudes of $M_z(t)$ obtained at different values of φ [16]. However, any averaging method with the phase change cannot completely eliminate them because the time development of $M_z(t)$ includes the components of the oscillations independent of φ as is recognized by a more detailed analysis of Eq. (21). When we pay attention to the TQ nutation itself, it is convenient to use the PM(II). The upper figure of Fig. 7 shows an example of the TQ nutation signal observed by the PM(II). We cannot show how the PM(II) considerably decreases the higher frequency oscillations, but can infer that the component of the magnetization along the second effective field ω_e^*/γ changes into that along the RF field fairly smoothly owing to the tail of the PM pulse.

When the frequency ω_2 slightly shifts from ω_{20}, the Hamiltonian $\mathscr{H}_7$ is modified as

$$\mathscr{H}_7 = -\delta I_z - \omega_3 I_x + \bar{\mathscr{H}}_d^{(7)}, \tag{29}$$

with $\delta = \omega_e^* - 2\omega_2$. In this case, the TQ nutation is caused around the effective field $\sqrt{\delta^2 + \omega_3^2}/\gamma$ at an angle η with the transverse field ω_3/γ $(\tan\eta = \delta/\omega_3)$. If the frequency ω_2 varies under the condition of the constant amplitude of the LF field, δ is approximately given by $\frac{1}{2}(\omega_1/\omega_{20} + 3)(\omega_{20} - \omega_2)$, which is roughly three times as large as the difference $\omega_{20} - \omega_2$. The time development of $M_z(t)$ produced under the Hamiltonian in Eq. (29) is also described by Eq. (21) by replacing $\xi_r(r = x, y, z)$ by $\xi_r^{\#}$, ω_3 by $\sqrt{\delta^2 + \omega_3^2}$, and $\mathscr{H}_d^{\dagger}$ by the secular part of $\bar{\mathscr{H}}_d^{(7)\#} = \exp(-i\eta I_y)\bar{\mathscr{H}}_d^{(7)}\exp(i\eta I_y)$, where the angles $\xi_r^{\#}(t)$'s satisfy the relation

$$\exp(-i\eta I_y)V(t)I_zV(t)^{-1}\exp(i\eta I_y) = \cos\xi_x^{\#}(t)I_x + \cos\xi_y^{\#}(t)I_y + \cos\xi_z^{\#}(t)I_z. \tag{30}$$

We here ignore the higher frequency oscillations around ω_2, $3\omega_2$, and $5\omega_2$ for simplicity. The dependences of the initial angle $\xi_x^{\#}(0)$ on φ and η indicate that $\xi_x^{\#}(0)$ can vary almost over the range of π rad by changing φ and η. At $\varphi = 0$, $\xi_x^{\#}(0) = \pi/2 - \alpha - \theta - \eta$, and therefore, $\xi_x^{\#}(0)$ can be zero for a certain value of η. The upper figure of Fig. 8 shows the experimental time development of $M_z(t)$

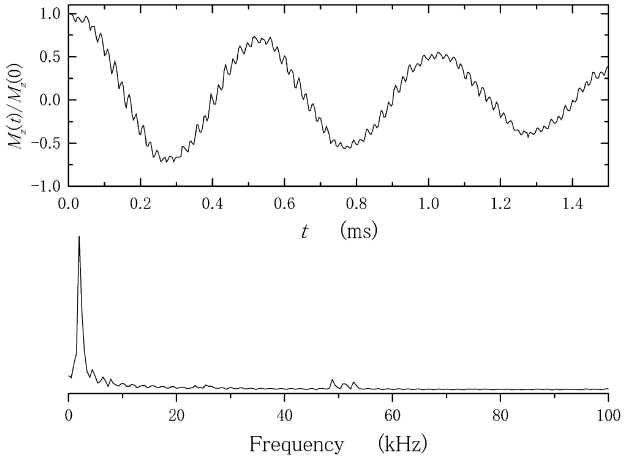

Fig. 7. Experimental time development of M_z at the exact TQ resonance observed with PM(II) and its Fourier spectrum. The experimental condition is $\omega_1/2\pi = 65.0$ kHz, $\omega_{20}/2\pi = 25.45$ kHz, $\varphi = 0$, and $\varphi_m = 1.058$ rad. The nutation frequency measured is 2.02 kHz.

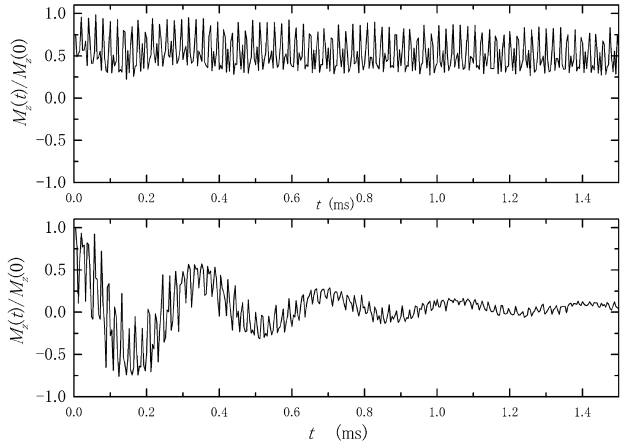

Fig. 8. Experimental time developments of M_z at TQ off-resonance. The upper trace is the behavior of M_z observed under $\xi_x^{\#}(0) \cong 0$, where the experimental condition is $\omega_1/2\pi = 65.0$ kHz, $\omega_{20}/2\pi = 26.2$ kHz, $\omega_2/2\pi = 25.4$ kHz, $\varphi = 0$, and $\varphi_m = 1.17$ rad (at $\omega_2/2\pi = 25.4$ kHz). The theoretically estimated values of $\delta/2\pi$ and $\omega_3/2\pi$ are 2.01 and 2.57 kHz, respectively. The lower one is that under $\xi_x^{\#}(0) \cong \pi/2$. The experimental condition is $\omega_1/2\pi = 65.0$ kHz, $\omega_{20}/2\pi = 26.26$ kHz, $\omega_2/2\pi = 25.80$ kHz, $\varphi = 55°$, and $\varphi_m = 1.15$ rad (at $\omega_2/2\pi = 25.80$ kHz). The estimated values of $\delta/2\pi$ and $\omega_3/2\pi$ are 1.32 and 2.62 kHz, respectively.

observed for $\xi_x^{\#}(0) \cong 0$, which indicates that almost the whole magnetization is along the field $\sqrt{\delta^2 + \omega_3^2}/\gamma$ in the triply rotating frame, where δ is comparable to ω_3 (see the figure caption of Fig. 8). It is possible to measure the relaxation time in the quadruply rotating frame by eliminating the higher frequency oscillations with a low pass filter, for example. The lower figure of Fig. 8 indicates the experimental result obtained for $\xi_x^{\#}(0) \cong \pi/2$. The oscillation appears to be a nutation signal at exact resonance though it is the phenomenon at the TQ off-resonance.

4.2. Contribution of the dipole interaction to the TQ nutation decay

For this study, the nutation was observed by averaging four magnitudes of $M_z(t)$ observed at $\varphi = n\pi/8$ $(n = 0, 1, 2, 3)$ by the PM(II), by which the higher frequency oscillations were almost eliminated. We measured the decay times T for various values of φ_m at $\omega_1/2\pi = 60, 65$, and 70 kHz by assuming an exponential decay ($e^{-t/T}$) as shown in Fig. 9 and confirmed that the φ_m dependence of T is consistent with that of the coefficient $|B - A|/2$ independent of ω_1/γ, and also, with the experimental result in Fig. 2 in [4]. The decay times T around φ_{m0} were much longer than those of the SQ magic angle rotary echo observed in the laboratory frame [17] and of the SQ magic angle nutation observed in the same original rotating frame as that of the TQ nutation. The longer decay time of the TQ nutation is explained by the differences in the coefficients of the

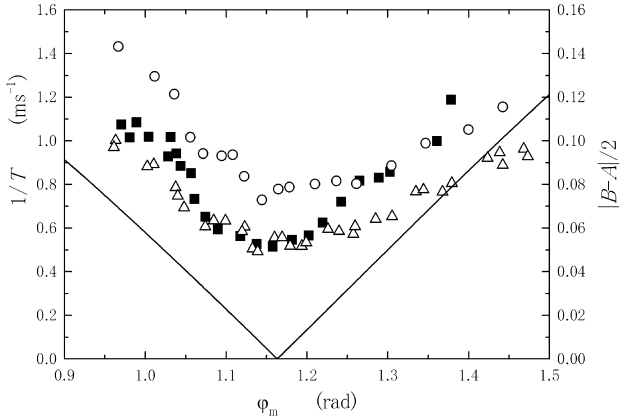

Fig. 9. φ_m dependences of the decay times T of the TQ nutations. The circles, the triangles, and the squares show the experimental values of T^{-1} measured at $\omega_1/2\pi = 60, 65$, and 70 kHz. The solid line is the theoretical curve of $|B - A|/2$. The result that the decay times T around $\varphi_m = \varphi_{m0}$ ($\cong 1.16322$ rad) are not as long as is expected from the theoretical curve is mainly due to the influence of the dipole interaction represented by the nonsecular part $\mathscr{H}_d^{\ddagger}$.

nonsecular parts of the dipole Hamiltonian [4]. The corresponding dipole Hamiltonians in the SQ resonances under the rotating wave approximation are also of the same forms as the right-hand sides of Eqs. (24), (26), and (27). The coefficients $\frac{1}{2}|3A + B|$ and $|C|$ of the nonsecular parts are 1 and $\sqrt{2}$ for the laboratory frame, and 1/2 and $1/\sqrt{2}$ for the rotating frame, which are larger than the corresponding values (2.44×10^{-3} and 0.23079) of the TQ resonance.

We finally consider the more general case including TQ off-resonance with $\bar{\mathscr{H}}_d^{(7)\#}$. The Hamiltonian $\bar{\mathscr{H}}_d^{(7)\#}$ is also written in the same form as Eq. (24) with the coefficients $A^{\#}$, $B^{\#}$, and $C^{\#}$ corresponding to A, B, and C in $\bar{\mathscr{H}}_d^{(7)}$. Therefore, the secular and the nonsecular parts of $\bar{\mathscr{H}}_d^{(7)\#}$ are given by the expressions similar to Eqs. (26) and (27). The coefficient of the secular part is

$$\tfrac{1}{2}(B^{\#} - A^{\#}) = \tfrac{1}{4}(A + B) + \tfrac{1}{4}(B - 3A)\cos 2\eta + \tfrac{1}{2}C \sin 2\eta. \tag{31}$$

We define the average angle $\bar{\xi}_x^{\#}$ of $\xi_x^{\#}(t)$ by

$$\cos \bar{\xi}_x^{\#} \equiv < \cos \xi_x^{\#}(t) >_{av} = \tfrac{1}{2} \sin\theta(\cos\alpha - 1)\cos\eta + \cos\theta \cos\alpha \sin\eta. \tag{32}$$

We assume that $\delta < 0$ at an infinitesimal value $\Delta\varphi_m$ of φ_m. Since the value of $\cos \bar{\xi}_x^{\#}$ is a function only of ω_1/ω_2 and φ_m, and the condition of $A^{\#} = B^{\#}$ gives a relation between ω_1/ω_2 and φ_m, the angle $\bar{\xi}_x^{\#}$ is determined only by φ_m under the condition that $A^{\#} = B^{\#}$, which is denoted by ξ_x^*. We here call the angle ξ_x^* a magic angle in the triply rotating frame. We can easily see from Eqs. (25), (31), and (32) that at $\varphi_m = \Delta\varphi_m$, the coefficients B and C are zero, and the magic angle ξ_x^* becomes equal to the well-known magic angle $\cos^{-1}(-1/\sqrt{3})$, where $\sin\theta \cong \theta$ and $\sin\alpha \cong \alpha$. As φ_m increases, the magic angle

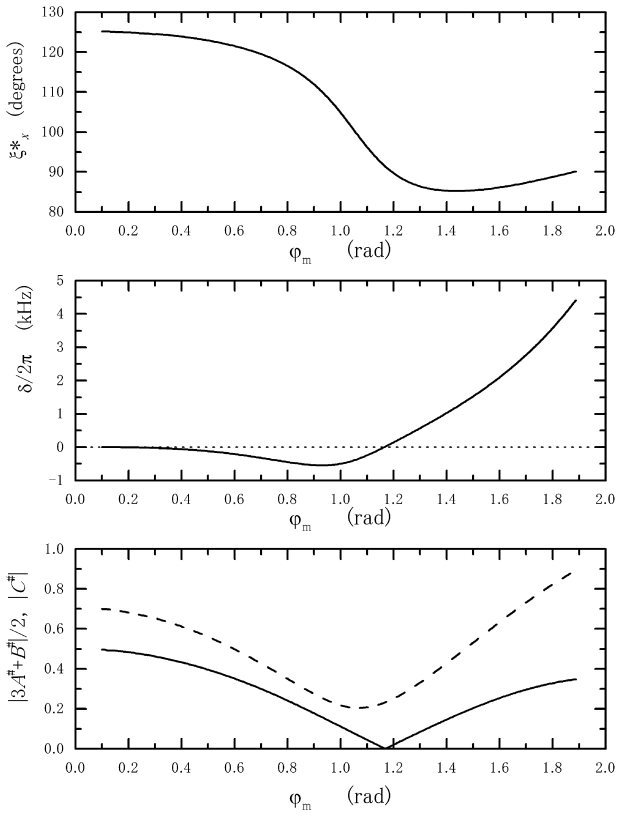

Fig. 10. Theoretical φ_m dependences of ξ_x^*, δ and the coefficients of the nonsecular parts obtained under the condition that $A^{\#} = B^{\#}$ in the case of $\delta < 0$ at $\Delta\varphi_m$. The top and the middle figures indicate that at $\delta = 0$, $\xi_x^* \cong 91.6°$. The solid and the dashed lines in the bottom figure are the curves of $|3A^{\#} + B^{\#}|/2$ and $|C^{\#}|$, respectively.

varies as shown in the top of Fig. 10. The middle and the bottom parts of Fig. 10 indicate that the longest decay time of the TQ nutation is expected almost at the exact resonance ($\delta = 0$), and then, the magic angle is near $\pi/2$.

In the case of $\delta > 0$ at $\Delta\varphi_m$, the magic angle becomes $\cos^{-1}(1/\sqrt{3})$ at $\Delta\varphi_m$. However, this kind of magic angle is not so important for the narrowing because the value of $\delta/2\pi$ in this case monotonously increases as φ_m increases, and is more than 5 kHz even in the range of φ_m in which the coefficients of the nonsecular parts become comparably small.

5. Concluding remarks

The present paper verifies the theory in Section 2 describing the TQ nutation and the narrowing effect in the two-level spin system. The time development of the spin-locked magnetization $M_z(t)$ indicates the TQ nutation signal accompanied by the higher frequency oscillations generally consisting of the six simple harmonic oscillations. The higher frequency oscillations owe to the fluctuation of the angle $\xi_x^{\#}(t)$ between the transverse field $\sqrt{\delta^2 + \omega_3^2}/\gamma$ and the RF field. The initial angle $\xi_x^{\#}(0)$ at $\varphi = 0$ can become 0 for an appropriate value of δ, and then, the whole magnetization is spin-locked by the field $\sqrt{\delta^2 + \omega_3^2}/\gamma$ in the triply rotating frame. It is expected that the decay of the magnetization along $\sqrt{\delta^2 + \omega_3^2}/\gamma$ presents the relaxation time in the quadruply rotating frame.

The modulation index $2\varphi_m$ of the PM is the key parameter controlling the conditions of the TQ resonance and the TQ nutation decay. At the exact resonance, the value of φ_m determines alone the angles θ and α, the ratios ω_1/ω_{20} and ω_3/ω_{20}, and the coefficients A, B, and C in $\bar{\mathscr{H}}_d^{(7)}$. Therefore, the secular part of $\bar{\mathscr{H}}_d^{(7)}$ vanishes at a particular value of $\varphi_m = \varphi_{m0}$, which is about 1.16322 rad. The decay time measured around φ_{m0} is much longer than those of the SQ magic angle rotary echo observed in the laboratory frame and of the SQ magic angle nutation observed in the same rotating frame as that of the TQ nutation under the condition that the rotating wave approximation is valid. The longer decay time of the TQ nutation is explained by the differences in the coefficients of the nonsecular parts of the dipole Hamiltonian.

The disappearance of the secular part is also possible at TQ off-resonance. We can define the magic angle in the triply rotating frame with the average angle ξ_x^* at which the secular part vanishes. At $\varphi_m = \Delta\varphi_m$, the magic angle ξ_x^* is equal to the well-known value $\cos^{-1}(-1/\sqrt{3})$ for $\delta < 0$ at $\Delta\varphi_m$ or $\cos^{-1}(1/\sqrt{3})$ for $\delta > 0$ at $\Delta\varphi_m$. The magic angle in the case of $\delta < 0$ at $\Delta\varphi_m$ is nearly equal to $\pi/2$ at the TQ exact resonance and important for the narrowing, but the other case is not so important.

The magic angle is in principle possible in the SQ exact resonance under the influence of the counter-rotating component. A theoretical φ_m dependence of the coefficient of the secular part of the relevant dipole Hamiltonian under the SQ exact resonance shows that the secular part disappears at $\varphi_m \cong 1.633$ rad. However, this is not practical because the strength of the LF field $\varphi_m\omega_2/\gamma$ for this value of φ_m becomes about 10 times as large as that of the RF field.

The narrowing effect of the TQ nutation will be useful if the TQ nutation signal is observed by one shot with a multiple pulse method, for example.

Acknowledgments

The authors are indebted to Mr. Takeo Ibe for his assistance in the experiments.

References

[1] W.I. Goldburg, M. Lee, Nuclear magnetic resonance line narrowing by a rotating rf field, Phys. Rev. Lett. 11 (1963) 255–258;

M. Lee, W.I. Goldburg, Nuclear-magnetic-resonance line narrowing by a rotating rf field, Phys. Rev. A 140 (1965) 1261–1271.

[2] See for example E.R. Andrew, The narrowing of NMR spectra of solids by high-speed specimen rotation and the resolution of chemical shift and spin multiplet structures for solids, in: J.W. Emsley, J. Feeney, L.H. Sutcliffe (Eds.), Progress in Nuclear Magnetic Resonance Spectroscopy, vol. 8, Pergamon Press, New York, 1971, pp. 1–39.

[3] See for example M. Mehring, High Resolution NMR Spectroscopy in Solids, Springer-Verlag, Berlin, New York, 1976.

[4] H. Hatanaka, N. Tabuchi, New line-narrowing effect in triple-quantum resonance in a two-level NMR system, J. Magn. Reson. 155 (2002) 119–122, doi:10.1006/jmre.2001.2492.

[5] I. Solomon, Étude de la relaxation en résonance magnétique par la méthode de précession forcée transitoire, C.R. Acad. Sci. 248 (1959) 92–94.

[6] S.R. Hartmann, E.L. Hahn, Nuclear double resonance in the rotating frame, Phys. Rev. 128 (1962) 2042–2053.

[7] J.H. Shirley, Solution of the Schrodinger equation with a Hamiltonian periodic in time, Phys. Rev. 138 (1965) B979–B987;
S. Stenholm, Saturation effects in RF spectroscopy I. General theory, J. Phys. B 5 (1972) 878–889;
S. Stenholm, Saturation effects in RF spectroscopy II. Multiple quantum transitions, J. Phys. B 5 (1972) 890–895;
Y. Zur, M.H. Levitt, S. Vega, Multiphoton NMR spectroscopy on a spin system with $I = 1/2$, J. Chem. Phys. 78 (1983) 5293–5310.

[8] F. Ahmad, R.K. Bullough, Theory of the Bloch–Siegert shift, J. Phys. B 7 (1974) L275–L280.

[9] S. Swain, Analytic expressions for the positions of the longitudinal and transverse resonances in radio-frequency spectroscopy, J. Phys. B 7 (1974) 2363–2367.

[10] R. Boscaino, F.M. Gelardi, G. Messina, Double-quantum nutations in a two-level spin system, Phys. Rev. B 33 (1986) 3076–3082;
R. Boscaino, G. Messina, Double quantum coherent transients in a two-level spin system: a vectorial model, Physica C 138 (1986) 179–187.

[11] See for example C.P. Slichter, Principles of Magnetic Resonance, Springer, Berlin, New York, 1990.

[12] A. Abragam, The Principles of Nuclear Magnetism, Oxford Univ. Press, Oxford, 1961.

[13] F. Bloch, A. Siegert, Magnetic resonance for nonrotating fields, Phys. Rev. 57 (1940) 522–527.

[14] J.G. Powles, J.H. Strange, Zero time resolution nuclear magnetic resonance transients in solids, Proc. Phys. Soc. 82 (1963) 6–15.

[15] A.G. Redfield, Nuclear magnetic resonance saturation and rotary saturation in solids, Phys. Rev. 98 (1955) 1787–1809.

[16] N. Tabuchi, H. Hatanaka, Rotating frame analog of spin-locking and spin–lattice relaxation in the doubly rotating frame, J. Magn. Reson. 148 (2001) 121–125, doi:10.1006/jmre.2000.2217.

[17] H. Kessemeier, W.-K. Rhim, NMR line narrowing by means of rotary spin echoes, Phys. Rev. B 5 (1972) 761–768.